SCALING OF THE REYNOLDS STRESS IN WALL-BOUNDED FLOWS

T.-W. Lee and J.E. Park
Department of Mechanical and Aerospace Engineering
Arizona State University
Tempe, Arizona, USA
attwl@asu.edu

ABSTRACT

Scaling of the Reynolds stresses has been sought by many researchers, since it provides a template of universal dynamical patterns across a range of Reynolds numbers. Various statistical and normalization schemes have been attempted, but without complete or convincing similarity properties. Our prior work on the transport processes in wall-bounded flows point toward self-similarity in the gradient space, where the first and second derivatives of the Reynolds stress components exhibit universal scaling across the entire boundary layer. Scaling characteristics and physical implications are discussed in this work.

Introduction

Scaling of the mean velocity (U) profiles in turbulent flows serves a useful function of collapsing the momentum structure. Then, expansion or "stretching" by an appropriate multiplicative factor recovers the profile at other Reynolds numbers, e.g. in boundary-layer and free-jet flows. Similar patterns are sought in turbulence structures, for example the diagonal components of the Reynolds stress tensor (u'^2, v'^2, w'^2). In addition to replicating the profiles at arbitrary Reynolds numbers, complete scaling would lead to insights on the dynamics and origins of the turbulent flow structure,

Attempts at finding similarity in the turbulence profiles in wall-bounded flows have been mostly at the "surface" level, i.e. in the root variables (e.g. u'^2 as a function y+) and their higher statistical moments (Marusic et al., 2010, Hu et al., 2020). Measurements and DNS show progressions in the u'^2 profiles with increasing Reynolds number (Figure 1), wherein the peak increases in magnitude while moving closer to the wall (Graham et al., 2016; Iwamoto et al., 2002; Mansour et al., 1998; Marusic et al., 2010). Interestingly, when plotted in the inner coordinates (y+) the peak location stays nearly constant approximately at y+ = 15 (Moser et al., 1999; Marusic et al., 2010; Keirsbulck et al., 2012). Although some sectional scaling rules have been reported (Smits et al., 2021; Buschmann and Gad-el-Hak, 2007), self-similarity over the entire flow domain has been elusive.

The attached eddy hypothesis is a dynamical model of the turbulence structure in the so-called "logarithmic region". In that regard, it also suggests a method to generate a universal profile, although the transposition from the hypothesis to the actual statistics are not as straightforward (Hu et al., 2020). The model assumes that a hierarchy of eddies near the wall would lead to a logarithmic dependence for the normal components of the Reynolds stress (Marusic et al., 2010; Marusic and Monty, 2019; Hu et al., 2020), but this argument is applicable only in the descending segment of the profile (Adrian, 2010; Marusic and Monty, 2019). In the gradient (d/dy+) space, u'^2 =-Alog(y+)+B would correspond to $du'^2/dy+=-A/y+$, which is plotted in Figure 2 along with DNS data from Iwamoto et al. (2002) and Graham et al. (2016) for turbulent channel flows. In Figure 2, overlap of the logarithmic distribution with the $du'^2/dy+$ profiles is rather brief, while noting the fact that log scale is used for y+. Whether or not the attached eddy hypothesis and its dynamical prescriptions are correct in the logarithmic region, it is not of much use in scaling or explaining other prominent features in u'^2 (e.g. near-wall peak shapes) or its relations with other Reynolds stress components.

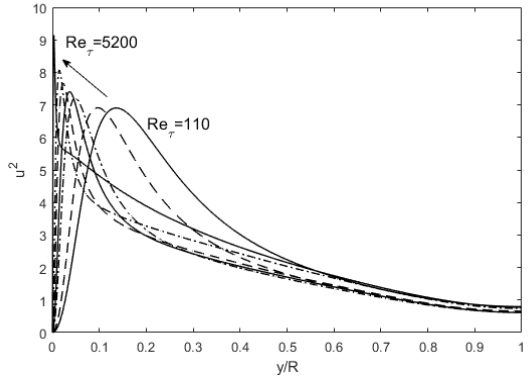

Figure. 1. Progression of u'^2 profiles with increasing Reynolds number in channel flows. The DNS data from Iwamoto et al. (2002) and Graham et al. (2016) are used.

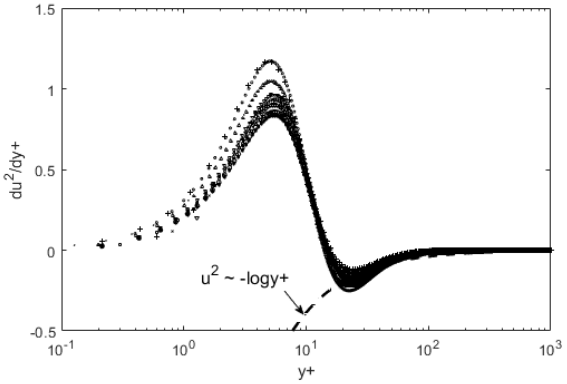

Figure. 2. A look at the gradient structure, $du'^2/dy+$. Logarithmic dependence (attached eddy model) is plotted as a dashed line. The DNS data from Iwamoto et al. (2002) and Graham et al. (2016) are used.

Figure 2 actually starts to illustrate the turbulence dynamics involving u'^2. When plotted as gradients ($du'^2/dy+$), the profiles now become self-similar, with a common zero-crossing point at $y+ \sim 15$ (peak location for u'^2). With respect to this peak location, both the near-wall positive $du'^2/dy+$ (u'^2 ascending) and mid-layer negative slope ($du'^2/dy+ < 0$) sections now exhibit self-similarity for the entire range of Reynolds number (Re_τ= 110-5200) plotted. These scaling characteristics distinctly point to the advantages of examining turbulence structure in the gradient (d/dy+) space. In this work, we show that scaling can be found at the first and second gradient ($d/dy+$, $d^2/dy+^2$) levels for the Reynolds stress components. Implications on the origin of such turbulence structure in wall-bounded flows are also discussed, along with transport relationships between u'^2, v'^2, and $u'v'$.

Scaling of the Reynolds Stresses

If we take the first gradient of u'^2 profiles, then self-similarity is found across a large range of Reynolds numbers and different wall-bounded (flat-plate and channel) flows, as was shown in Figure 2. The fixed peak location ($y+\sim 15$) serves as a pivot (zero-crossing) point for positive and negative segments. Also, the maxima and minima in the gradients vary with the Reynolds number (Lee, 2021a; Lee, 2021b), asymmetrically (steeper for the positive segments) but both in a monotonic manner so that scaling factors can be introduced to collapse the profiles. The maximum u'^2 variation with the Reynolds number has been correlated using DNS data (Keirsbulck et al., 2012). Similarly, maxima (peak) and minima (nadir) for $du'^2/dy+$ can be tabulated as a function of the Reynolds number. We have used the DNS data of Iwamoto et al. (2002) and Graham et al. (2016) for channel flows (Re_τ= 110-5200), and also of Spalart (1998) for boundary-layer flow over a flat plate (Re_τ=300 – 1410), for the turbulence profiles including evaluations of the maxima and minima in $du'^2/dy+$ (Figure 2). The profiles in Figure 3 are thus scaled in the y+ axis through the d/dy+ operation, and normalized by the absolute values of the extrema (maxima/minima), $(du'^2/dy+)_{ext}$, in the vertical direction. Upon doing so, we can see that in Figure 3 the collapse of the profiles is nearly perfect, universal across the Reynolds number for both the channel and boundary-layer flows, and covers the entire flow width. Segmented, partial scaling rules are no longer necessary with the universal gradient (d/dy+) scaling. We should be also able to deduce the turbulence dynamics from this self-similarity characteristic, as discussed in the next section.

Similar patterns are observed for v'^2 and $u'v'$, except at the *second-gradient* level (Figures 4 and 5). As shown in Figures 3-5, the gradient profiles all collapse when properly normalized by the peak/nadir heights of the second gradients. Thus, a profile at a reference Reynolds number can be used to reconstruct u'^2, v'^2, or $u'v'$ at any other Re_τ, by appropriate "stretching" (Lee, 2021a; Lee, 2021b).

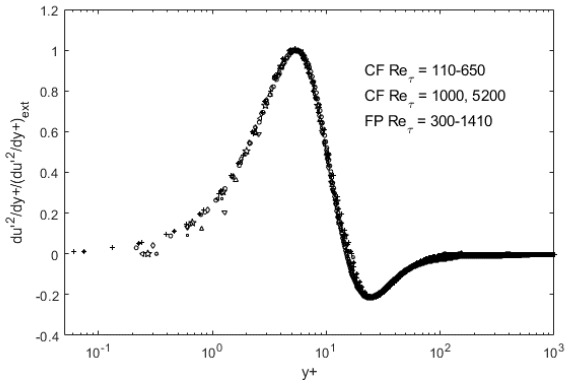

Figure 3. Scaled $du'^2/dy+$ profiles for channel (CF) and boundary-layer (FP) flows. The DNS data from Graham et al. (2016) and Spalart (1998) are used.

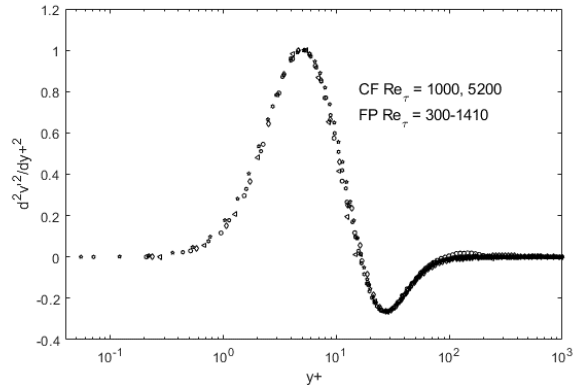

Figure. 4. . Scaled $d^2v'^2/dy+^2$ profiles for channel (CF) and boundary-layer (FP) flows. The DNS data from Graham et al. (2016) and Spalart (1998) are used. The data have been normalized by the absolute values of the maxima and minima, similar to Figure 3.

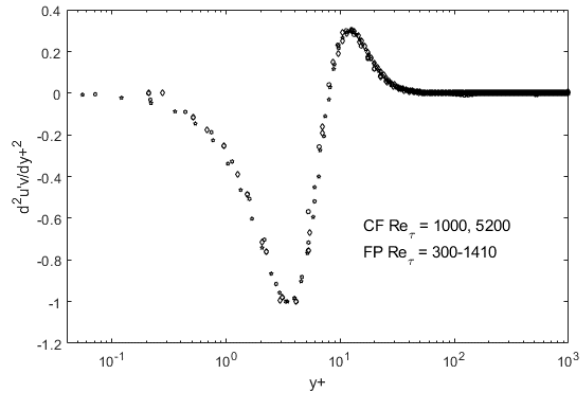

Figure 5. Scaled $d^2u'v'/dy+^2$ profiles for channel (CF) and boundary-layer (FP) flows. The DNS data from Graham et al. (2016) and Spalart (1998) are used. The data have been normalized by the absolute values of the maxima and minima, similar to Figure 3.

The results in the above figures (Figs. 3-5) show that the gradient scaling is complete over the flow width and universal for wall-bounded flows for a large range of Reynolds numbers. Recent examinations of the turbulence profiles in adverse pressure-gradient boundary layers indicate that the self-similarity also exists in other turbulence configurations (Lee and Park, 2023).

Origin of the Turbulence Structure

The self-similarity exhibited in the previous section provokes thoughts as to the reason for this dynamical scaling. Let us first consider u'^2 structure. The progression in the u'^2 with increasing Re number seemed fairly irregular in Figure 1, involving an increasingly sharp peak near the wall at high Reynolds numbers with a bend of the slope in the descending portion. However, when plotted in the d/dy+ space, self-similarity emerges, with the y+ ~ 15 marking the zero-crossing (peak location). The near-wall structure is scaled with respect to this peak location. y+ is the spatial variable normalized by the viscous length scale, and it contracts the observed $du'^2/dy+$ profile near the wall where the viscous force is the most significant. With increasing Reynolds number, the u'^2 peak height increases with a fixed peak location (y+~15). Therefore, y+ ~ 15 represents the viscous length scale (Figure 6) corresponding to the region where this near-wall dynamics occurs. The fluctuation velocity ($u'=u'_{rms}$) is constrained by the wall boundary condition and the viscous effect in the near-wall region, and this creates a steep gradient toward the peak u'^2 at a given Reynolds number. This is the origin of the near-wall peak structure, and it collapses when scaled by the "viscous dissipation gradient (d/dy+)". Once this gradient is set, then the centerline (channel flows) or the free-stream (boundary-layer) condition requires the downward, or negative slope starting from u'^2 peak. This results in the self-similarity in the $du'^2/dy+$ profiles, with y+=15 serving as the pivot point, as was shown in Figure 3.

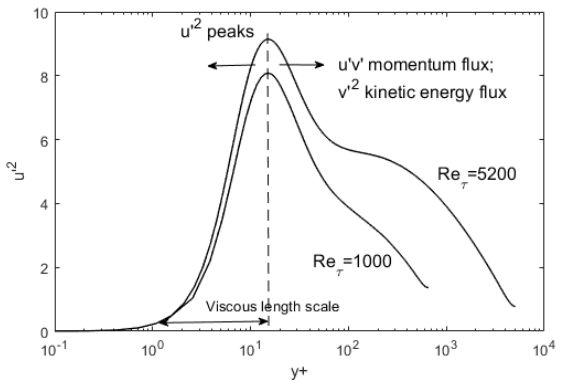

Figure 6. Dynamics of the dissipation scaling in wall-bounded flows.

Once the u'^2 profile is generated in this manner, the maximum (peak) u'-momentum or u'^2-kinetic energy near the wall constitutes an asymmetry or an overshoot that must be transported away. The gradient transport in the momentum balance (for turbulence fluctuation) dictates that the fluxes be maximum at this point. The physical interpretation is illustrated in Figure 6, and the corresponding dynamical relationships for the turbulence transport (Lee, 2021a) have been developed for the Reynolds stress components (Eqs. 1-3 below). In this perspective, the excess u'-momentum near the wall is transported by $du'^2/dy+$ and $du'v'/dy+$ flux terms (Eq. 1). Net pressure force is written with $P \sim \rho v'^2$, and the second derivatives ($d^2/dy+^2$) are the viscous force. Also, d/dx is transformed to d/dy+ through the displacement effect (Lee, 2021a). Similarly, excess turbulence momentum, v', is re-distributed through $du'v'/dy+$ flux term, and balanced by the pressure and viscous forces in Eq. 2. Eq. 3 represents the transport equation for u'^2 kinetic energy. Thus, momentum and energy are two facets of turbulence fluctuations, and excess concentrations lead to fluxes away from the peaks. The above logical sequence results in the $du'v'/dy+$ and $dv'^2/dy+$ flux terms attaining their respective maximum near y+ ~ 15. If we go back to the scaled figures of Figures 4 and 5, we see that the $u'v'$ and v'^2 are scaled at the $d^2/dy+^2$ space with y+ ~ 10 and 15 acting respectively as the anchor or inflection point, i.e. maximum in the fluxes of u'-momentum ($du'v'/dy+$) or v'-momentum ($dv'^2/dy+$). Once this zero-crossing is set, then the positive and negative peaks on either side again scale with the Reynolds number. Upon proper normalization all collapse onto a unitary trace at the second-gradient level (Figures 4 and 5).

u'-momentum:

$$\frac{d(u'v')}{dy} = -C_{11}U\frac{d(u'^2)}{dy} + C_{12}U\frac{dv'^2}{dy} + C_{13}\frac{d^2u'}{dy^2} \quad (1)$$

v'-momentum:

$$\frac{d(v'^2)}{dy} = -C_{21}U\frac{d(u'v')}{dy} + C_{22}U\frac{dv'^2}{dy} + C_{23}\frac{d^2v_{rms}}{dy^2} \quad (2)$$

u'^2-kinetic energy:

$$\frac{d(u'^3)}{dy} = -C_{31}\frac{1}{U}\frac{d(u'v'\cdot u')}{dy} + C_{32}\frac{1}{U}\frac{d(v'\cdot u'v')}{dy} + C_{33}\frac{1}{U}\left(\frac{du'}{dy}\right)^2 \quad (3)$$

In summary, the Reynolds stress components are visualized as transport variables following the same conservations of momentum and energy, when cast in a coordinate frame moving at the local mean velocities. In contrast to the Eulerian analysis which includes both the mean and fluctuating components, the transport analysis for a control volume moving at the local mean velocity (U, V) leads to a succinct set of flux equations for the Reynolds stress components (u'^2, $u'v'$, and v'^2). The dynamical equations have been developed and verified in previous works (Lee, 2020; Lee, 2021a; Lee, 2021b), and assist in visualizing the turbulence flux dynamics and resulting structure. The form of the transport equations reveals that the Reynolds stresses originate from the local momentum balance, decoupled from the mean velocities, and that the components ($u'v'$, u'^2, and v'^2) are inter-related.

Transport of the Reynolds Stress

Above observations are consistent and quantified with the momentum (Eqs. 1 and 2) and u'^2 kinetic energy (Eq. 3) transport balances. This set of turbulence transport equations has been validated for a range for flow geometries, including

wall-bounded flows (Lee, 2021a), pipe flows with swirl (Lee, 2020b), and adverse pressure-gradient boundary layer flows (Lee ad Park, 2023). Examples are shown in Figure 7. First, Eq. 1 is used to determine the Reynolds shear stress gradient (du'v'/dy) for boundary-layer flow over a flat plate. Current theory is plotted as a solid line, and DNS data of Spalart 1988) in symbols. The steep decrease in u'v' is translated into a large negative slope region near the wall, with the (negative peak) again corresponding to the zero-cross in du'v'/dy plot. Individual contributing terms in Eq. 1 are also individually plotted as transport (first term on RHS), pressure (second), and viscous (third). We saw in Figures 1 and 2 that u'^2 has a large peak (production) near the wall, and this results in the corresponding transport and viscous effects, which results in nearly exactly matched du'v'/dy profile in Figure 7 when coupled with the pressure term. Far from the wall, each of the terms asymptotes to the free-stream boundary condition, again nearly perfectly replicating the observed du'v'/dy gradient. Thus, no coercive or complex modelling or arguments are needed to determine the Reynolds stresses. They are physically, succinctly and accurately prescribable through this new theoretical perspective.

Above observations suggest that the Reynolds shear stress (u'v') is very remotely, if at all, related to the mean velocity gradient (dU/dy). Also, turbulence momentum flux terms (u'^2 and v'^2) need to be introduced to correctly balance the u'v' transport. Similar observations and confirmations the turbulence flux dynamics through Eqs. 2 and 3 are made in Figures 7(b) and 7(c), respectively, for v'^2 and u'^2 (or u'^3) for channel flows. With momentum fluxes, pressure and viscous force terms, we have Eqs. 1-3 for the Reynolds stress components (du'v'/dy, dv'^2/dy and du'^3/dy), as validated in previous works (Lee, 2020a, Lee, 2020b, Lee, 2021a, Lee, 2021b, Lee and Park, 2023). Then, by coupling Eqs. 1, 2 an 3 with the RANS (Reynolds-averaged Navier-Stokes) equation, we can fully prescribe the turbulent flow field (Lee, 2020b).

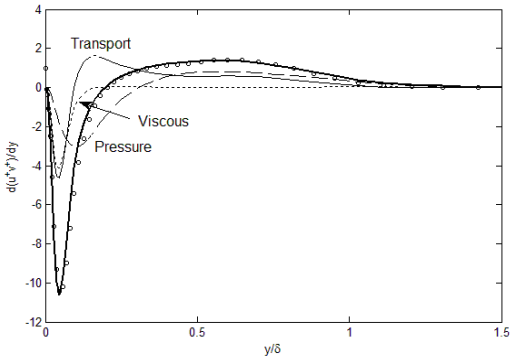

(a)

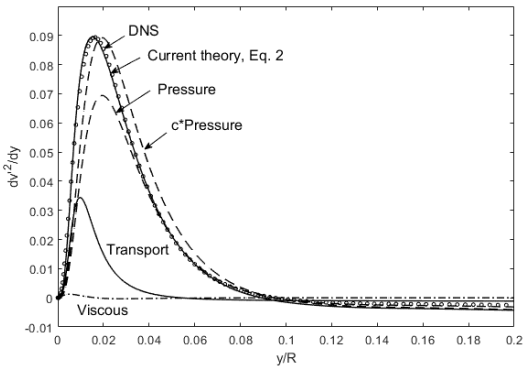

(b)

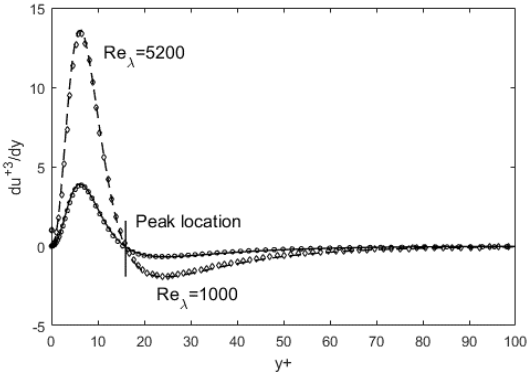

(c)

Figure 7. Validation of the turbulence flux equations (Eqs. 1-3) in wall-bounded flows: (a) u-momentum balance (Eq. 1) leading to an expression for du'v'dy for boundary-layer flow over a flat plate (DNS data from Spalart (1988) are plotted as small symbols); (b) v'-momentum balance (Eq. 2) for channel flows (DNS data from Graham et al., (2016) are plotted as symbols); and (c) u'^2-kinetic energy balance (Eq. 3) for channel flows (DNS data from Graham et al., (2016) are plotted as symbols).

Concluding Remarks

The dissipation scaling in the turbulence structure is discussed, along with its dynamical origins. In the gradient space (d/dy+, d^2/$dy+^2$), the self-similarity is complete and universal. Considerations of the gradient transport (flux) also lead to the turbulence flux equations (Eqs. 1-3), which are validated (e.g. Lee, 2021a). The flux equations allow insights and "visualization" of the turbulence flow structure and self-similar patterns, and in conjunction with the RANS equation, represent a viable solution for wall-bounded turbulent flows.

REFERENCES

Adrian, R.J., "Closing in on models of wall turbulence," Science **329**, 155–156 (2010).

Graham, J., Kanov, K, Yang, X.I.A., Lee, M.K., Malaya, N, Lalescu, C.C., Burns, R., Eyink, G, Szalay, A, Moser, R.D., and Meneveau, C., 2016, A Web Services-accessible database of turbulent channel flow and its use for testing a new integral wall model for LES, Journal of Turbulence, 17(2), 181-215.

Hu, B., Xiang, I.A.Y. and Zheng X., 2020, Wall-attached eddies in wall-bounded turbulent flows, Journal of Fluid Mechanics, Vol. 194, pp. 15-44.

Iwamoto, K., Sasaki, Y., Nobuhide K., 2002, Reynolds number effects on wall turbulence: toward effective feedback control, International Journal of Heat and Fluid Flows, 23, 678-689.

Keirsbulck, L., Fourrie, G., Labraga, L., and Gad-el-Hak, M., 2012, Scaling of statistics in wall-bounded turbulent lows, Comptes Rendus Mecanique, 340, 420-433.

Lee, T.-W., 2020a, Lagrangian Transport Equations and an Iterative Solution Method for Turbulent Jet Flows, Physica D, 132333.

Lee, T.-W., A Generalizable Theory of the Reynolds Stress, 2020b, arXiv:2006.01634.

Lee, T.-W., 2021a, Dissipation scaling and structural order in turbulent channel flows, Physics of Fluids, 33, 5, 055105.

Lee, T.-W., 2021b, Asymmetrical Order in Wall-Bounded Turbulent Flows, Fluids, 6(9), 329.

Lee, T.-W., 2023, Dynamics and scaling of the Reynolds stress in adverse pressure-gradient turbulent boundary layer flows, arXiv:2310.19723, also to be submitted to a journal.

Mansour, N.N., Kim, J. and Moin, P., 1998, Reynolds-stress and dissipation-rate budgets in a turbulent channel flow, Journal of Fluid Mechanics, Vol. 194, pp. 15-44.

Marusic, I., McKeon, B.J., Monkewitz, P.A., Nagib, H.M., Smits, A.J., and Sreenivasan, K.R., 2010, Wall-bounded turbulent flows at high Reynolds numbers: Recent advances and key issues, Physics of Fluids, 22, 065103.

Marusic, I. and Monty, J.P., 2019, Attached eddy model of wall turbulence, Annual Review of Fluid Mechanics, 51:49-74.

Moser, Robert D., John Kim, and Nagi N. Mansour, 1999, Direct numerical simulation of turbulent channel flow up to Re_t= 590, Physics of Fluids, 1999, 11,4, pp. 943-945.

Smits, A.J., Hultmark, M., Lee, M., Pirozzoli, S., and Wu, X., 2021, Reynolds stress scaling in the near-wall region of wall-bounded flows, Journal of Fluid Mechanics, 926, A31.

Spalart, P.R., 1988, Direct simulation of a turbulent boundary layer up to Re=1410, Journal of Fluid Mechanics, Vol. 187, pp. 61-77.

Tennekes, H. and Lumley, J.L., A first course in turbulence, MIT press, 1972.

APPENDIX: Notes on the Turbulence Flux Equations (Eqs. 1-3)

The key idea in arriving at Eqs. 1 -3 is the consideration of momentum and energy fluxes for a control volume moving at the local mean velocity (U, V), as shown in Figure A1. For example, we can visualize ourselves riding in a submersible that is travelling at the local mean velocity. Opening of the hatches will not rush the fluid inward from the mean relative motion, since it is zero. Only the fluctuating velocity components will perform the transport. Then, u' momentum is transported by u' itself in the streamwise, and by v' in the cross-stream direction (Figure A1). This will result in the momentum balances in Eqs. 1 and 2. We can consider a similar flux balance for the u'^2 kinetic energy (Eq. 3).

A new transform of d/dx to d/dy transform is introduced in all of the transport equations. This is based on the displacement concept (Lee, 2021a) where a control volume moving in the boundary layer would see a lateral shift in the vertical profile (Figure A2). Due to this displacement effect, d/dx is converted to a d/dy term with the mean velocity acting as the proportionality constant (Eq. 4): the faster the mean motion (U) the more the vertical shift. For channel flows bounded by walls, there are no displacement effects; however, a "probe transform" bearing the same functional result is derived in Lee (2021b). This transform is what makes the transport equations (Eqs. 1-3) work, as validated in Figure 7 and in prior works (e.g. Lee, 2021a).

$$\frac{d}{dx} \rightarrow \pm C_{ij} U \frac{d}{dy} \qquad (4)$$

C_{ij} is a constant with the unit, ~ $1/U_{ref}$. The +/- sign depends on the flow geometry, i.e. the direction of displacement relative to the reference point. Implicit in this transform idea is that the both the vectors (u', v') and scalars (pressure, u'^2) are displaced or transformed in this manner. The coefficient matrix, C_{ij}, is assigned for different terms in Eqs. 1-3: C_{i1}'s are for the lateral transport, C_{i2}'s modify the pressure term while absorbing the effect of density, and C_{i3} are the kinematic viscosity, n (C_{13} and C_{23}) or 2n (C_{33}). As is well known, there will be larger displacement effects at higher Reynolds numbers since u'^2 and other variables will become progressively more skewed. Thus, as expected we find a Reynolds-number dependence $C_{11} = 6.86 \times 10^{-5} Re_\lambda^{\frac{1}{2.5}}$ for channel flows (Lee, 2020b).

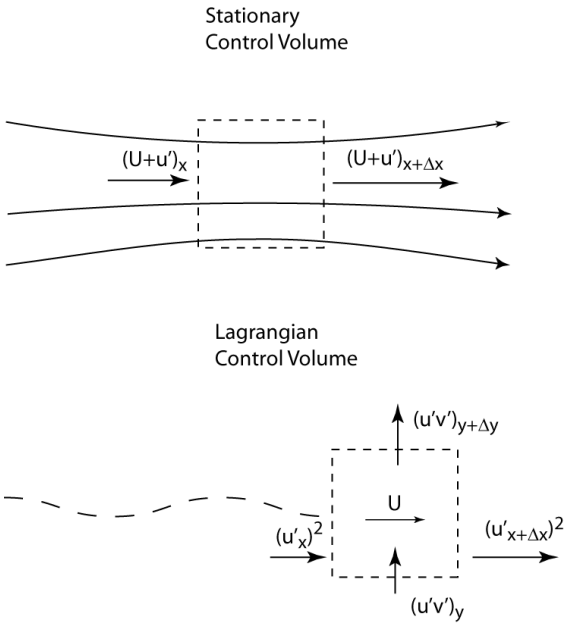

Figure A1. Eulerian vs/ Lagrangian control volume analysis.

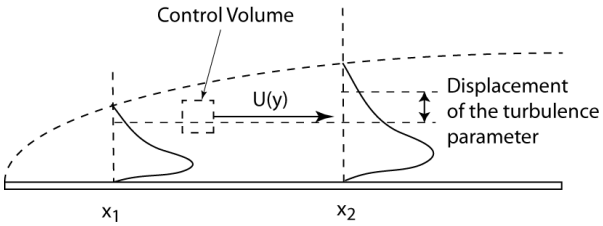

Figure A2. Displacement effect leading to the d/dx to d/dy transform.

For the pressure terms, we use

$$P \approx -\rho v'^2 \qquad (5)$$

For channel flows, this relation is exact (Tenneke and Lumley, 1972), derivable from the y-component of the RANS, and we apply it as an approximation for boundary layer flows with and without adverse pressure gradient.

The u^2-transport equation (Eq. 3) contains the dreaded triple correlation(s). For the Lagrangian flux, a hypothesis is used for the triple correlations similar to a previous work (Lee, 2020a; Lee, 2020b), and validated with DNS data.

$$\frac{d(u'^2 v')}{dy} \approx \frac{d(u' \cdot u' v')}{dy}, \quad \frac{d(u' v'^2)}{dy} \approx \frac{d(v' \cdot u' v')}{dy}, etc. \qquad (6)$$

This differentiation rule decomposes the triple product in terms of existing variables, and leads to accurate results for u'^2 and v'^2 profiles.

Probe Transform

For channel flows, the flow is bounded and there is no displacement of the turbulence variables as one travels in the streamwise direction. However, the Galiean transform can be performed at any line of motion, and if we choose a slightly mis-directed path (U* and v*) for the control volume as shown in Figure A3, we obtain the same transform as shown below. In Figure A1, x* and y* axes are aligned in the same direction as U* and v*, respectively.

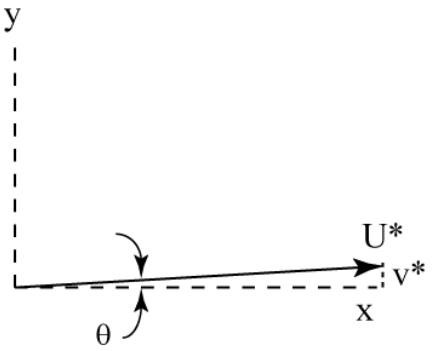

Figure A3. Off-set line of motion for the control volume, for "probing" the d/dy gradient.

For a small angle, q << 1, v* <<U and $U* \approx U$. Then,

$$\frac{\partial}{\partial x} = \frac{1}{cos\theta}\frac{\partial}{\partial x*} \approx \frac{\partial}{\partial x*} \qquad (7)$$

$$\frac{\partial}{\partial y} = \frac{1}{cos\theta}\frac{\partial}{\partial y*} \approx \frac{\partial}{\partial y*} \qquad (8)$$

For variable, f, we have

$$\frac{\frac{\partial f}{\partial y*}}{\frac{\partial f}{\partial x*}} \approx \frac{\frac{\partial f}{\partial y*}}{\frac{\partial f}{\partial x*}} = tan\theta = \frac{v*}{U*} \approx \frac{v*}{U} \qquad (9)$$

Thus, using this offset transform, we obtain

$$\frac{\partial f}{\partial x} = \frac{U*}{v*}\frac{\partial f}{\partial y} \approx C_1 U \frac{\partial f}{\partial y} \qquad (10)$$

C_1 is a constant in the order and unit of v*.